Bar-mode instability suppression in magnetized relativistic stars

L. Franci[1], R. De Pietri[1], K. Dionysopoulou[2] and L. Rezzolla[2,3]

[1] Dipartimento di Fisica e Scienze della Terra, Università di Parma and INFN, Parma, Italy
[2] Max-Planck-Institut für Gravitationsphysik, Albert-Einstein-Institut, Golm, Germany
[3] Institut für Theoretische Physik, Frankfurt am Main, Germany

E-mail: `luca.franci@fis.unipr.it`

Abstract. We show that magnetic fields stronger than about 10^{15} G are able to suppress the development of the hydrodynamical bar-mode instability in relativistic stars. The suppression is due to a change in the rest-mass density and angular velocity profiles due to the formation and to the linear growth of a toroidal component that rapidly overcomes the original poloidal one, leading to an amplification of the total magnetic energy. The study is carried out performing three-dimensional ideal-magnetohydrodynamics simulations in full general relativity, superimposing to the initial (matter) equilibrium configurations a purely poloidal magnetic field in the range $10^{14} - 10^{16}$ G. When the seed field is a few parts in 10^{15} G or above, all the evolved models show the formation of a low-density envelope surrounding the star. For much weaker fields, no effect on the matter evolution is observed, while magnetic fields which are just below the suppression threshold are observed to slow down the growth-rate of the instability.

1. Introduction

Differentially rotating neutron stars (NSs) are subject to the so-called $m = 2$ dynamical bar-mode instability for non-radial axial modes with azimuthal dependence $e^{im\phi}$ ($m = 1, 2, ...$), when the instability parameter $\beta \equiv T/|W|$ (i.e. the ratio between the rotational kinetic energy T and the gravitational binding energy W) exceeds a critical value. The bar-mode instability in differentially rotating magnetized NSs has already been studied in the Newtonian case by Camarda et al. [1], suggesting that the effect of magnetic fields on the emergence of the instability is not likely to be very signicant unless when NSs are born very highly magnetized.

In this work, we investigate if the presence of magnetic fields can affect the onset and development of this kind of instability in full general relativity, as well as the role played by the magnetic braking to possibly suppress the instability.

Our study is motivated by the potential implications that strong magnetic fields may have for astrophysical scenarios and for gravitational wave astronomy. In particular, during the last decade a general consensus has formed that long Gamma-Ray Bursts (GRBs) arise from the collapse of massive stars while short GRBs, most likely, from neutron star mergers. A key ingredient for both these categories of astrophysical phenomena is the formation of magnetic structures that could power the high-speed particle jets associated with GRBs [2].

We choose to evolve different equilibrium relativistic stellar models that have already been studied in the non-magnetized case by Baiotti et al. [3], so that their behavior against the bar-mode instability is already known and fully understood when no magnetic fields are present.
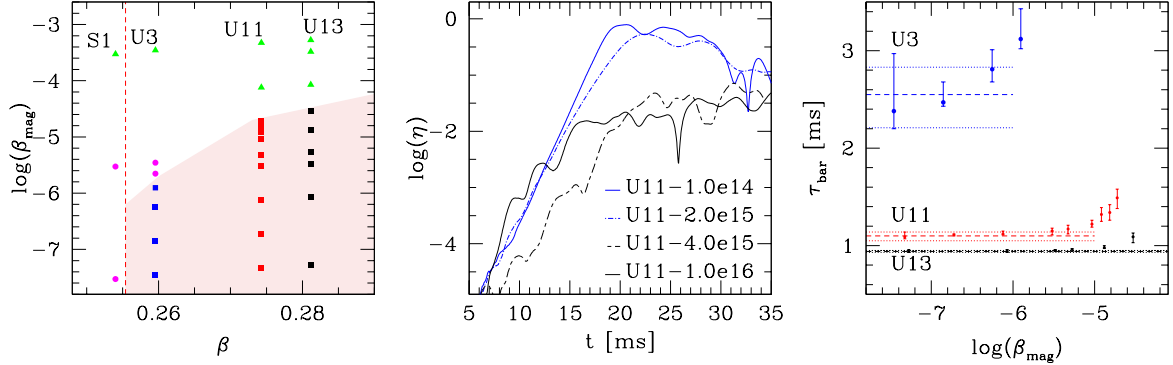
Figure 1. (Left panel): parameter space (β, β_{mag}) with the initial values of these two quantities for all the simulated models: the models inside the red shaded region turned out to be still matter-unstable even when a magnetic field is present. (Central panel): time evolution of the distortion parameter η for model U11 for four different values of the seed poloidal magnetic field strength. We use blue lines for matter-unstable models and black lines for the stable ones. (Right panel): growth-time τ_{bar} of the bar-mode instability versus the initial values of β_{mag}. The dashed lines represent the values in the non-magnetized cases while the dotted lines stand as error bars.

2. Initial data

The initial data for our simulations are computed as stationary equilibrium solutions of axisymmetric relativistic stars that are rapidly differentially rotating. In particular, we assume the non-uniform j-law angular velocity distribution

$$\Omega_c - \Omega = \frac{1}{\hat{A}^2 R_e^2} \left[\frac{(\Omega - \omega) r^2 \sin^2 \theta e^{-2\nu}}{1 - (\Omega - \omega)^2 r^2 \sin^2 \theta e^{-2\nu}} \right] , \tag{1}$$

where R_e is the coordinate equatorial stellar radius, the coefficient $\hat{A}$ is a measure of the degree of differential rotation, while ω and ν are metric components in spherical coordinates.

A seed poloidal magnetic field is added to these initial equilibrium models as a perturbation by introducing a purely toroidal vector potential $A_\phi = A_b \left(\max(p - p_{\mathrm{cut}}, 0) \right)^2$, where p_{cut} is 4% of the maximum initial pressure ($p_{\mathrm{cut}} = 0.04 \ \max(p(0))$) and A_b is chosen in such a way so that it corresponds to the maximum of the initial magnetic field on the (x, y) plane $B^z_{\mathrm{max}}|_{t,z=0}$.

The equilibrium models considered here have been calculated using a relativistic polytropic equation of state $p = K \rho^\Gamma$ with $K = 100$ and $\Gamma = 2$, in analogy with previous works in the literature. In particular, to better find out the changes to the bar-mode dynamics induced by the presence of a magnetic field, we focused our attention on a sequence of models having a fixed constant amount of differential rotation $\hat{A} = 1$ and a constant rest mass $M_0 \simeq 1.5 \ M_\odot$, which were already studied in the non-magnetized case in [3]. All the features of these models are then described in further detail in Tab. I of [3] and here we use the notation therein reported. For the present study, we selected the three models which were better discussed therein, namely models U3, U11 and U13, where U3 is the closest to the threshold for the onset of the bar-mode instability and U13 is almost the fastest rotating equilibrium model which can be obtained for this sequence at constant barionic mass (see the left panel of Fig. 1, where the threshold is indicated with a red dotted line corresponding to $\beta = 0.255$).

Indeed, all the simulated initial models are represented in the left panel of Fig. 1, where they are identified in terms of the initial values of the two parameters (β, β_{mag}), defined as $\beta \equiv T/|W|$ and $\beta_{\mathrm{mag}} \equiv E_{\mathrm{mag}}/(T + |W|)$, respectively. Here, T is the rotational kinetic energy, W the gravitational binding energy and E_{mag} the total magnetic energy. Hereafter, we will refer
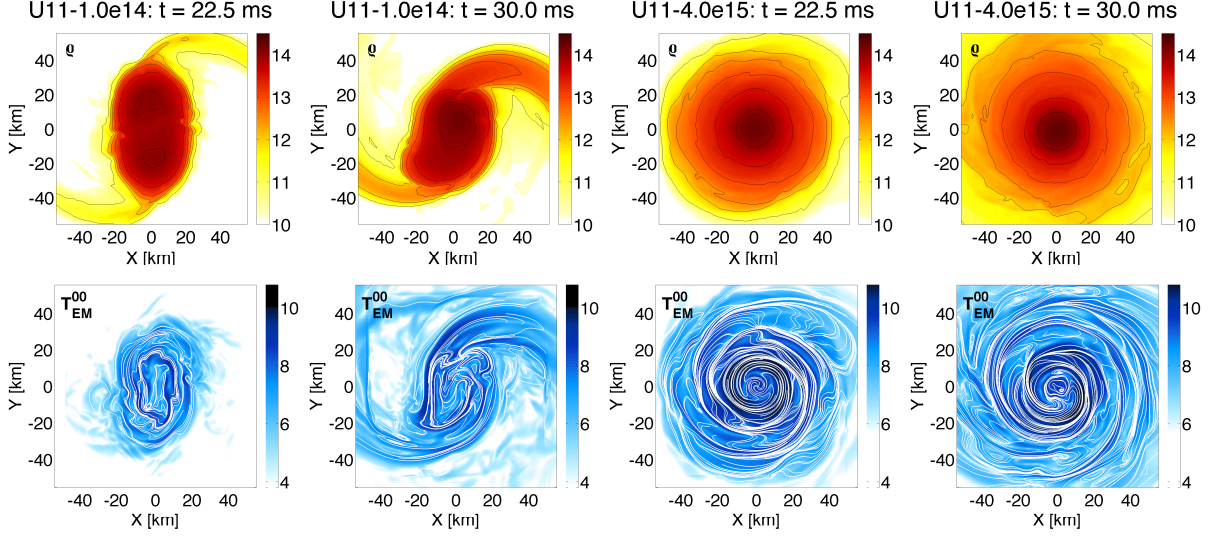
Figure 2. (Top panels): snapshots of the rest-mass density ρ on the (x, y) plane at $t = 22.5$ and 30.0 ms for model U11 with two different seed magnetic field strengths: $B_{\max}^z|_{t,z=0} = 1.0 \times 10^{14}$ G for model U11-1.0e14 (left panels) and $B_{\max}^z|_{t,z=0} = 4.0 \times 10^{15}$ G for U11-4.0e15 (right panels). The color code is defined in terms of $\log_{10}(\rho)$ where ρ is in cgs units (g/cm³). Additionally, isodensity contours are shown for $\rho = 10^{11}$, 10^{12}, 5×10^{12}, 10^{13}, 5×10^{13} and 10^{14} g/cm³; (Bottom panels): snapshots of the local magnetic energy T_{EM}^{00} on a horizontal plane at $z \simeq 1.5$ km for the same two models at the same steps during the evolution. Additionally, magnetic field lines are drawn in white. The color code is defined in terms of $\log_{10}(T_{\mathrm{EM}}^{00}/c^2)$ where T_{EM}^{00}/c^2 is in cgs units (g/cm³).

to a particular evolved stellar model by using the notation Uxx-yy, where xx is the initial model and yy denotes the maximum initial magnetic field strength (U11-1.0e14 refers to a U11 model with a super-imposed purely poloidal magnetic field such that $B_{\max}^z|_{t,z=0} = 1.0 \times 10^{14}$ G).

3. Computational setup

The simulations reported here have been performed using the general-relativistic magnetohydrodynamics (GRMHD) code WhiskyMHD described in [5] and which is based on the Cactus computational toolkit. The gravitational fields are evolved using the BSSNOK formulation with the same gauge conditions and parameters as in [3], while the GRMHD equations are solved using a high-resolution shock-capturing scheme based on the piecewise parabolic (PPM) reconstruction and the Harten-Lax-van Leer-Einfeldt (HLLE) approximate Riemann solver. For all the simulations discussed here we have used a grid structure with four refinement levels, an outer boundary located at $L \simeq 100\ M_{\odot}$ ($\simeq 150$ km) and finest resolution of $\Delta x = 0.375\ M_{\odot}$ ($\simeq 0.5$ km). With this setting the outer boundary is far enough to have all the dynamics happening inside the computational domain, while the used resolution is already able to capture the dynamics of the magnetic field (see [4]).

4. Results

For each unstable model (U3, U11 and U13) we have performed a number of simulations adding an initial purely poloidal magnetic field around the typical value of the field strengths expected for magnetars (that is of the order of 10^{15} G) and, indeed, in the range from 1.0×10^{14} G to 1.0×10^{16} G. Much stronger initial magnetic fields are quite unlikely to be realistic, while weaker fields seems to have no effects at all on the dynamics of the bar-mode instability.
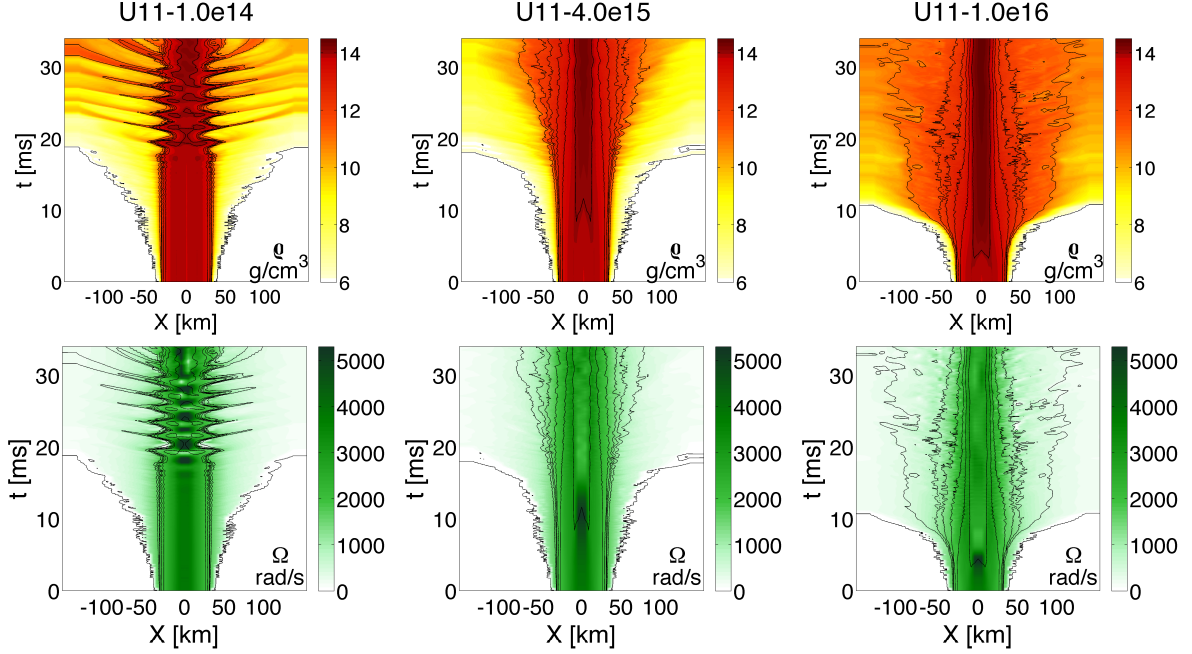
Figure 3. Evolution of the rest-mass density ρ (top row) and the angular velocity Ω (bottom row) along the x axis for models U11-1.0e14 (left panels), U11-4.0e15 (central panels) and U11-1.0e16 (right panels). The panels show the color-coded quantities embedded in a space-time diagram with the coordinate time t on the vertical axis. Additionally, on top of all diagrams isodensity contours are shown for $\rho = 10^6$, 10^{11}, 10^{12}, 5×10^{12}, 10^{13}, 5×10^{13} and 10^{14} g/cm^3.

The dynamics of the bar-mode instability ($m = 2$ mode) is studied following the evolution of the distorsion parameter $\eta = (\eta_+^2 + \eta_\times^2)^{1/2}$, which is defined in terms of the matter quadrupole moment in the xy directions through the quantities $\eta_\times = 2\, I^{xy}/(I^{xx} + I^{yy})$ and $\eta_+ = (I^{xx} - I^{yy})/(I^{xx} + I^{yy})$. In the central panel of Fig. 1 we show how the dynamics of η is affected by different choices of the initial magnetic field strength: in unstable models, like model U11-1.0e14, this parameter shows an exponential growth (whose growth time, τ_{bar}, can be easly measured).

In particular, regarding the bar-mode instability, we draw the conclusion that there are three distinct behaviors corresponding to different seed magnetic fields.

Indeed, we observe no effects at all on the dynamics of the instability up to a certain magnetic field strength (namely, $B^z_{\max}|_{t,z=0} \lesssim 2.0 \times 10^{14}$ G for model U3, 4.0×10^{14} G for model U11 and 8.0×10^{14} G for model U13), since both the growth time and the frequency of the m=2 matter mode do not vary within the accuracy they can be computed with (see the left panels of Fig. 2 and Fig. 3 and the right panel of Fig. 1). For higher field strengths we observe a gradual slowdown in the development of the instability, since the magnetic field lines are frozen into the fluid and the differential rotation has to drag them together with the matter implying that the instability growth time τ_{bar} is higher for higher initial values of β_{mag} (see the right panel of Fig. 1). The models that are still matter-unstable, even when a magnetic field is present, are represented with squares in the left panel of Fig. 1 showing the parameter space (β, β_{mag}).

Going to much higher fields we reach a threshold value above which the instability is completely suppressed and the deformation no longer develops. This threshold on the magnetic field still depends on the initial model adopted, being higher than about 6.0×10^{14} for model U3, 2.0×10^{15} for model U11 and 2.4×10^{15} for model U13 (see Fig. 1).

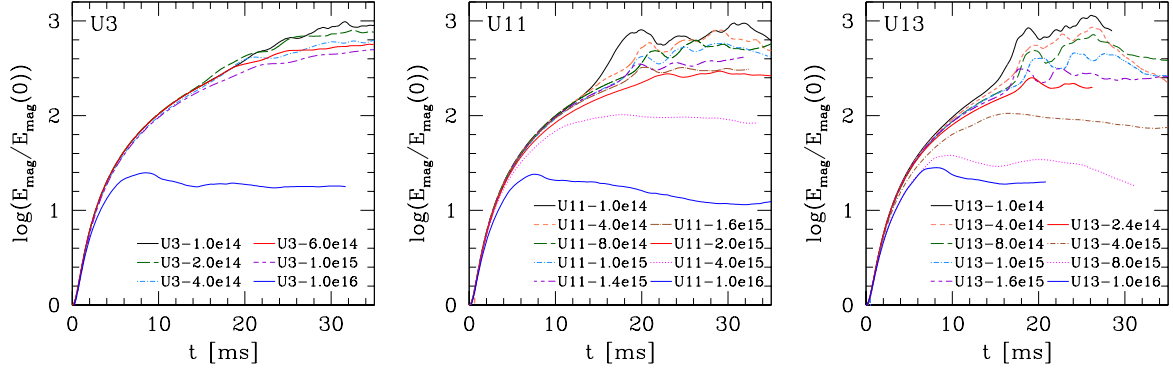Besides, for very strong seed magnetic fields, we also observe changes on the density and

Figure 4. Time evolution of the total magnetic energy E_{mag} normalized to its initial value for the three models which are unstable in the non-magnetized case (`U3`, `U11` and `U13`) corresponding to a wide range of seed magnetic fields from $B^z_{\max}|_{t,z=0} = 1.0 \times 10^{14}$ G to 1.0×10^{16} G. We use a black solid line to depict the less magnetized case, a blue solid line to indicate the most magnetized case and a red solid line for the last unstable model just before the suppression of the bar-mode instability due to the presence of the magnetic field.

angular velocity profiles of the stellar models, so in the end of the evolution we obtain a much more compact configuration that is nearly uniformly rotating and surrounded by a very low density envelope which is still differentially rotating (see the right panels in Fig. 2 for model `U11`). This is consistent with the expectation that magnetic braking is transferring angular momentum from the core to the outer layers. Models that are matter-stable are indicated by circles in Fig. 1, while the ones that also exhibit the above-mentioned expansion of the outer layers due to the presence of the magnetic field are represented with triangles.

Taking a closer look at the magnetic field evolution for all seed magnetic fields, we observe that magnetic field lines wind due to differential rotation, and hence a development and linear growth of a toroidal component take place, with a consequent amplification of the total magnetic energy of about two orders of magnitude or even more (see Fig. 4). Moreover, we observe a further exponential growth of both poloidal and toroidal components during the matter-unstable phase, whose nature still needs to be investigated.

After having studied how the magnetic field affects the onset and development of the bar-mode instability, we turned to investigate whether there are effects on the dynamics of models which are known to be stable in the non-magnetized case. Once again, this was achieved by superimposing a purely poloidal seed magnetic field allowing the magnetic field strength to take two values; $B^z_{\max}|_{t,z=0} = 1.0 \times 10^{15}$ G and $B^z_{\max}|_{t,z=0} = 1.0 \times 10^{16}$ G.

Regarding the distribution of matter we observe negligible effects when $B^z_{\max}|_{t,z=0} = 1.0 \times 10^{15}$ G. Only for model `S1`, which is very close to the threshold for the onset of the dynamical instability (see the left panel of Fig. 1), we observe some minor changes. More specifically, the density profile turns from a toroidal initial configuration to a nearly standard one with its maximum quite close to the z-axis. In stable models with $B^z_{\max}|_{t,z=0} = 1.0 \times 10^{16}$ G, instead, we observe the same behavior already described for highly magnetized models, namely the outer layers expand forming an envelope of much lower density around the initial stellar model.

5. Conclusions

We have analyzed how the presence of magnetic fields can affect the development of the bar-mode ($m = 2$) instability in relativistic differentially rotating stellar models with a seed poloidal magnetic field in the range $10^{14} - 10^{16}$ G. In order to do that we have performed 3D magneto-hydrodynamical simulations coupled to the Einstein equations.

For all the models studied we have found, as expected, a sudden formation and linear growth of a toroidal component of the magnetic field (in a twisted configuration) that rapidly overcomes the original poloidal one and an amplification of the total magnetic energy to up to almost three orders of magnitude.

For relativistic stellar models that are bar-mode unstable, we have observed almost no effects on the bar-mode dynamics due to magnetic fields of the order of 10^{15} G or below. For stronger magnetic fields the growth time of the instability increases and the bar deformation appears to partially stall. Moreover, magnetic fields stronger than about 10^{15} G are able to completely suppress the instability and to change the density and angular velocity profiles of the stellar models, eventually leading to a final configuration where the star has almost uniform rotation and is surrounded by a very low density envelope.

he same evolution is realized also for relativistic stellar models that are stable against bar-mode deformations for seed magnetic fields of the order of 10^{16} G. Moreover, we note that the presence of magnetic fields does not alter the dynamics in stable models up to field strengths of the order of about 10^{15} G.

The overall conclusion is that only magnetic fields of the order of 10^{15} G or above seem to be able to suppress the purely hydrodynamical instability and so it is quite unlikely that in realistic astrophysical situations such a suppression due to the presence of magnetic fields might occur. Indeed, the general picture discussed in [1] applies also in the non Newtonian regime.

References

[1] Camarda K., Anninos P., Fragile P. C. and Font J. A. 2009 *Astrophys. J.* **707** 1610-22
[2] Rezzolla L., Giacomazzo B., Baiotti L., Granot J. and Kouveliotou C. 2011 *Astrophys. J. Lett.* **732** L6
[3] Baiotti L., De Pietri R., Manca G. M. and Rezzolla L. 2007 *Phys. Rev.* D **75** 044023
[4] Franci L., De Pietri R., Dionysopoulou K. and Rezzolla L., *arXiv:1308.3989*.
[5] Giacomazzo B., Rezzolla L. and Baiotti L., *Phys. Rev.* D **83** 044014.